



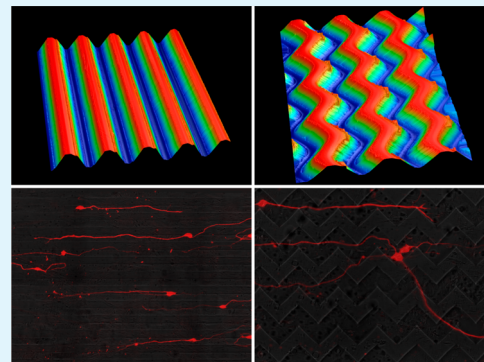
# Neural Pathfinding on Uni- and Multidirectional Photopolymerized Micropatterns

Bradley W. Tuft,<sup>†</sup> Linjing Xu,<sup>‡</sup> Scott P. White,<sup>†</sup> Alison E. Seline,<sup>‡</sup> Andrew M. Erwood,<sup>‡</sup> Marlan R. Hansen,<sup>‡</sup> and C. Allan Guymon\*,<sup>†</sup>

<sup>†</sup>Department of Chemical and Biochemical Engineering, University of Iowa, Iowa City, Iowa 52242, United States, United States

<sup>‡</sup>Department of Otolaryngology, University of Iowa Hospitals and Clinics, Iowa City, Iowa 52242, United States, United States

**ABSTRACT:** Overcoming signal resolution barriers of neural prostheses, such as the commercially available cochlear implant (CI) or the developing retinal implant, will likely require spatial control of regenerative neural elements. To rationally design materials that direct nerve growth, it is first necessary to determine pathfinding behavior of de novo neurite growth from prosthesis-relevant cells such as spiral ganglion neurons (SGNs) in the inner ear. Accordingly, in this work, repeating 90° turns were fabricated as multidirectional micropatterns to determine SGN neurite turning capability and pathfinding. Unidirectional micropatterns and unpatterned substrates are used as comparisons. Spiral ganglion Schwann cell alignment (SGSC) is also examined on each surface type. Micropatterns are fabricated using the spatial reaction control inherent to photopolymerization with photomasks that have either parallel line spacing gratings for unidirectional patterns or repeating 90° angle steps for multidirectional patterns. Feature depth is controlled by modulating UV exposure time by shuttering the light source at given time increments. Substrate topography is characterized by white light interferometry and scanning electron microscopy (SEM). Both pattern types exhibit features that are 25 μm in width and 7.4 ± 0.7 μm in depth. SGN neurites orient randomly on unpatterned photopolymer controls, align and consistently track unidirectional patterns, and are substantially influenced by, but do not consistently track, multidirectional turning cues. Neurite lengths are 20% shorter on multidirectional substrates compared to unidirectional patterns while neurite branching and microfeature crossing events are significantly higher. For both pattern types, the majority of the neurite length is located in depressed surface features. Developing methods to understand neural pathfinding and to guide de novo neurite growth to specific stimulatory elements will enable design of innovative biomaterials that improve functional outcomes of devices that interface with the nervous system.



**KEYWORDS:** photopolymerization, pattern, microsurface topography, contact guidance, neural prosthesis, neurite

## 1. INTRODUCTION

The interface between a biomaterial and biological tissue is a complex, dynamic microcellular environment that dictates the ultimate performance of a clinical device or material. Continuing advances in materials science, micro- and nano-fabrication, and tissue engineering enable design of 2D and 3D constructs that allow researchers to probe and even drive specific cell-material interactions along this crucial interface.<sup>1</sup> For example, many studies illustrate that stem cell phenotype can be manipulated by altering the material characteristics of the nascent environment.<sup>2–4</sup> Further, biomaterial mechanical or chemical properties and surface morphologies can be tailored to address requirements of a given cellular niche to improve functional outcomes of the biomaterial. Because of the innate ability that neurons have to explore and respond to their microenvironment—via de novo neurite growth during development or regeneration—and due to their importance in sensory, motor, and autonomic functions, they are the focus of substantial effort in cell-biomaterial interaction studies.<sup>5–8</sup>

In particular, a diverse array of methods is employed to direct the outgrowth of regenerative neural processes to span and repair damage in the peripheral nervous system. Nerve autographs remain the gold standard in clinical settings for these types of repairs, but recent advances in fabrication of multifaceted synthetic nerve conduits enable satisfactory neural regeneration and functional recovery even across large nerve gaps (>10 cm).<sup>8</sup> Typical methods used to direct regenerative neurite outgrowth include aligned microfibers,<sup>9</sup> bioactive molecule patterning,<sup>10–13</sup> parallel micro- and nanochannel morphology,<sup>14,15</sup> diffusion gradients of chemo-attractants,<sup>16</sup> electrical fields,<sup>17</sup> intraluminal guidance structures,<sup>18</sup> and oriented glial cells.<sup>19</sup> The primary objective of many neurite guidance studies is to effect maximal unidirectional outgrowth to bridge large gaps typical of nerve injuries. However, analogous neurite guidance techniques may also serve to

**Received:** March 17, 2014

**Accepted:** June 9, 2014

**Published:** June 9, 2014

address spatial resolution challenges that limit functional outcomes of neural prostheses by directing neurite growth to specific stimulatory elements.<sup>20–22</sup>

Neural prostheses electrically stimulate neural tissue to restore or augment remaining motor and sensory functions of neural pathways that were lost or damaged due to disease or physical trauma. Partly due to spatial resolution limitations, prostheses fail to recapitulate the detailed interactions of neural networks and subsequently fail to precisely simulate motor and sensory signaling. For example, retinal prosthesis simulation is limited to a few sensory pixels due, in part, to electrical signal overlap among target neurons in the retina caused by spatial separation of stimulating electrodes from the neural tissue.<sup>22</sup> The cochlear implant (CI), which is currently the only sensory prosthesis in routine clinical use, enables basic speech perception but suffers from comparable spatial signaling limitations. Nonspecific excitation of spiral ganglion neurons (SGNs) within the cochlea precludes simulation of high fidelity tonal information for the user. Subsequently, CI patients struggle with complex auditory stimuli such as voice comprehension in noisy environments and music appreciation.<sup>23,24</sup>

Driving regenerative neural processes into closer spatial proximity of specific stimulating electrodes would allow for lower current trigger thresholds that would reduce problematic signal overlap, enable higher stimulatory specificity, and perhaps lead to greater precision in both signal input and biological functional output.<sup>25–31</sup> Moreover, since the nervous system depends on location specific signaling, similar spatial resolution limitations are anticipated for any device that interfaces with the nervous system. Consequently, determining neural pathfinding behavior in response to directional cues and precisely directing spatial regeneration will be crucial to realize the functional potential of next-generation neural prostheses.

Among the variety of methods reported to orient neurite outgrowth, directing cell-material interactions using engineered surface topography is of particular interest due to the stability, reproducibility, and high degree of control over surface physical features inherent to the process. The most widely reported patterning techniques used to fabricate micro- and nanoscale actionable physical cues require a photopatterning step, that is, radiative exposure through a photomask, during the process due to the excellent spatial reaction control afforded by masked light exposure. Typically, variations of traditional photolithography accompanied by subsequent soft lithography casting of an elastomer over patterned silicon masters constitute the primary fabrication methods for cell contact guidance studies. For example, electron-beam lithography was used to fabricate nanoscale ridge and groove topography that caused epithelial cells to elongate and align on silicon oxide substrates with depths as small as 70 nm.<sup>32</sup> Soft lithography casting of poly(dimethylsiloxane) was used in conjunction with photolithography methods to generate microgrooved chitosan conduits that oriented Schwann cell growth and increased neurotrophin expression compared to smooth substrates.<sup>33</sup> Further, photo- and soft lithography are used to generate master templates with variations in pattern shape, ridge width, and groove depth to influence cellular behavior and spatial outgrowth.<sup>34,35</sup>

In place of traditional photo- and soft lithography patterning methods, direct photopatterning of 2D surfaces or 3D constructs via photofunctionalization or photo-cross-linking reactions has emerged as a prominent alternative production

platform for cell-material interaction studies. Patterning materials in this way avoids use of expensive or highly reactive reagents required for traditional photolithography methods and is often accomplished in fewer processing steps. For example, a polyfluorene derivative was directly photopatterned on a poly(ethylenimine) substrate by spatially controlling cross-linking reactions prior to washing steps to generate cyto-adhesive and nonadhesive stripes.<sup>36</sup> Sequential photopolymerization steps were employed to create trapping and sorting wells to isolate single cells based on imaged phenotype.<sup>37</sup> Direct photopatterning methods have also been utilized to generate cyocompatible hydrogels with tunable degradation profiles<sup>38</sup> and with controlled microarchitecture<sup>39</sup> for tissue regeneration and cell encapsulation applications. Additionally, photopolymerization was used to surface functionalize polymeric substrates with immunosuppressive proteins to provide bioactive protection against activated T cells.<sup>40</sup> Each of these studies illustrates and utilizes specific advantages inherent to UV curing for cellular applications including excellent temporal and spatial control, mild reaction conditions, and few process steps.

In this contribution, we evaluate the turning capability and neural pathfinding behavior of neurites extending from SGNs on photopolymerized, multidirectional micropatterns with repeating 90° turns. The repeating turns are used as a topographical challenge that is compared with neural outcomes on unidirectional micropatterns and unpatterned substrates. SGNs are the sensory elements of the inner ear that enable the sense of hearing and are the target neurons that are electrically stimulated by a CI prosthesis. As we have previously reported, physical micropatterns for neural pathfinding studies are fabricated via direct photopolymerization while microfeature height and directionality are modulated by controlling UV exposure time and by photomasking techniques, respectively.<sup>33,41</sup> SGN neurite response to each pattern type are characterized by total length, alignment of neurite segments, ratio of process path on depressed features, and number of turning points. Because spiral ganglion Schwann cells (SGSCs) play a crucial supportive role for SGN regenerative neurites,<sup>42</sup> their alignment to each pattern type is also reported. Understanding neurite pathfinding behavior and developing methods to guide de novo neurite growth to specific stimulatory elements will enable design of innovative biomaterials that improve functional outcomes of devices that interface with the nervous system.

## 2. EXPERIMENTAL SECTION

**2.1. Glass Slide Methacrylation.** Glass slides were used as substrates for thin-film micropatterned polymers to facilitate cellular microscopy studies. To prevent polymer delamination from the substrate, standard glass slides (2.54 cm × 7.62 cm × 0.1 cm) were surface functionalized with a methacrylated silane coupling agent. The slides were first cleaned and oxidized with O<sub>2</sub> plasma for 3 min at 30 W RF power (PDC-001 Harrick Plasma Expanded Cleaner, Ithaca, NY) while under vacuum. Immediately following removal from the plasma chamber, the slides were immersed in a 1/100 v/v solution of 3-(trimethoxysilyl)propyl methacrylate (Aldrich) and *n*-hexane (Aldrich) overnight in a covered container at room temperature (~21 °C). After removal from the solution, each slide was rinsed with fresh hexanes and allowed to dry in a fume hood before being placed in a sealed container. Functionalized slides had a slightly translucent appearance following the hexane rinse. Methacrylated slides were used immediately after functionalization as substrates for polymerization.

**2.2. Micropatterned Substrate Fabrication.** Prepolymer mixtures of 40 wt % hexyl methacrylate (HMA, Aldrich) and 59 wt % 1,6-hexanediol dimethacrylate (HDDMA, Aldrich) were prepared with 1 wt % of 2,2-dimethoxy-2-phenylacetophenone (DMPA, BASF) as the photoinitiator. As shown in previous work, poly(HMA-co-HDDMA) supports attachment, survival, and growth of SGNs and SGSCs under *in vitro* conditions and works well for control and tuning of photopatterned physical guidance cues.<sup>41,43</sup> A volume of 20  $\mu\text{L}$  was pipetted onto the center of a methacrylated slide which was then covered with a 2.54 cm  $\times$  2.54 cm  $\times$  0.1 cm glass-chrome Ronchi rule photomask (Applied Image Inc., Rochester, NY) for parallel patterns, a repeating 90° angle mask (Nano-Fabrication Facility, University of Minnesota, MN) for angled patterns, or with a cut untreated glass slide of the same dimensions for unpatterned samples. Formulations spread evenly under the photomasks due to capillary forces between the glass plates. Samples were cured with a high-pressure mercury vapor arc lamp (Omnicure S1500, Lumen Dynamics, Ontario, Canada) with 365 nm at a light intensity of 16 mW/cm<sup>2</sup>. Light intensity was measured with a Cole-Parmer Series 9811 radiometer. The curing module was equipped with an 8 mm aperture  $\times$  50 mm length beam homogenizing fused silica light pipe (Edmund Optics) and a collimating lens (RLQ-1, Asahi Spectra). Microfeature amplitude was controlled by shuttering UV radiation at specific times. After polymerization, photomasks were removed from polymer surfaces and samples were washed with 95% ethanol to remove all residual monomer. Samples were allowed to air-dry before use.

**2.3. Micropattern Characterization.** **2.3.1. White Light Interferometry.** White light interferometry (Dektak Wyko 1100 Optical Profiling System, Veeco) was used to measure micropattern periodicity and absolute channel amplitude. Feature amplitude was reported as the difference between the maximum ridge value and the adjacent minimum groove value. Average feature height for a given polymerization condition was determined by measuring channel amplitude in nine different areas across each sample ( $n \geq 3$ ). Periodicity was measured as the distance between the highest points on adjacent ridges and was consistent with photomask band spacing. Measurements and 3D images were generated using *Vision* software associated with the instrument.

**2.3.2. Scanning Electron Microscopy.** Micropattern morphology was further characterized by scanning electron microscopy (SEM, S-4800, Hitachi). Polymer samples were mounted on aluminum SEM stubs using conductive silver paint to acquire top-down images. For cross-sectional images, glass substrates, and patterned polymers were fractured and then mounted vertically on specimen stages. The SEM specimen stage was angled using automated stage and software controls. Each polymer surface was sputter coated with gold prior to examination by SEM. Electron accelerating voltage was set at 2 kV.

**2.4. Cell Culture and SGN Survival.** Dissociated spiral ganglia (SG) cultures from P3-5 rat pups were prepared as previously described.<sup>44,45</sup> SGN cultures were maintained in Dulbecco's Modified Eagle Medium (DMEM) supplemented with N2 additives, 5% fetal bovine serum, neurotrophin-3 (NT-3, 50 ng/mL), and brain derived neurotrophic factor (BDNF, 50 ng/mL). Cultures were maintained in a humidified incubator with 6.5% CO<sub>2</sub> and fixed with 4% paraformaldehyde after 48 h. SGNs were plated on polymer substrates coated sequentially with poly-L-ornithine (100  $\mu\text{g}/\text{mL}$ ) and laminin (20  $\mu\text{g}/\text{mL}$ ). To quantify SGN survival, cultures were fixed with 4% paraformaldehyde at 4 °C for 20 min, permeabilized and blocked with 5% goat serum, 2% BSA, 0.1% Triton X in phosphate buffered saline (PBS), and immunostained with antineurofilament 200 (NF200) antibodies (1:400, Sigma-Aldrich) at 37 °C for 2 h. Alexa 488 conjugated secondary antibody (1:800, Invitrogen) was used to detect the primary antibody immunolabeling at room temperature for 1 h. Slides were coverslipped with ProLong Gold antifading reagent with DAPI (Life Technology) and sealed with nitrocellulose. Digital epifluorescent images were captured of the entire polymer surface using the scan slide application of Metamorph software (Molecular Devices, Silicon Valley, CA) on a Leica DMIRE2 microscope (Leica Microsystems, Bannockburn, IL) with a Leica DFC350FX digital camera. The total number of NF200-positive neurons with healthy

nuclei was counted for each polymer surface to determine SGN survival. Experiments were performed in duplicate and repeated at least three times.

**2.5. Immunostaining and Measurement of SGN Neurite Length and Branching.** Spiral ganglia cultures were immunostained with anti-S100 and antineurofilament 200 (NF200) antibodies (1:400, Sigma-Aldrich) to label Schwann cells and neurons, respectively.<sup>44</sup> Alexa 488 and Alexa 546 conjugated secondary antibodies (Life Technology) were used to detect primary antibody immunolabeling. Slides were coverslipped with ProLong Gold antifading reagent with DAPI (Life Technology). Digital epifluorescent images were captured on a Leica DMIRE2 microscope (Leica Microsystems, Bannockburn, IL) with Leica DFC350FX digital camera and Metamorph software (Molecular Devices, Silicon Valley, CA). Images of the entire well were captured using the scan slide feature in MetaMorph to eliminate imaging bias to short neurites. Spiral ganglion neuron (SGN) total neurite length was determined from digital images by measuring the longest process of 100 randomly selected neurites from each condition using the measurement tool in ImageJ (NIH, Bethesda, MD) as previously described.<sup>46</sup> Number of branches extending from SGN neurites was determined by averaging the total number of neurite bifurcations, including bifurcation of branches, for 100 randomly selected neurites from each condition.

**2.6. Determination of SGN Neurite Segment and SGSC Alignment.** Neurite alignment was measured as a distribution of angles relative to the horizontal plane of 10  $\mu\text{m}$  length neurite segments. At least 50 primary neurites from immunolabeled images were traced in ImageJ for each condition and X-Y distance data were analyzed using Matlab software. The angle of each segment was calculated relative to horizontal and all neurite angles were then binned in 10° segments from 10–90°. Random outgrowth would be evidenced by a relatively equal distribution among all angle bins. Strong alignment to the horizontal plane would be demonstrated by high population percentages in bins of 20° or less. Strong alignment to multidirectional patterns, that is, repeating 90° angle steps, would be evidenced by high percentages around 45° alignment angles since the pattern was rotated 45° during imaging.

SGSC alignment was determined as previously described by drawing the outline of the cell using ImageJ software and fitting an ellipse to the cell outline.<sup>41,43</sup> The angle made between the major axis of the ellipse and the pattern ( $\theta$ ) was measured in ImageJ.

**2.7. Characterization of SGN Neurite Tracking on Raised vs Depressed Features.** Preference of SGN primary neurites for the depressed or raised features of the polymer surface was determined by individual measurement of neurite segments on each feature, summing the length of neurite, and calculating the percentage of primary neurite length on each feature. Lengths were measured from immunolabeled images using the measurement tool in ImageJ (NIH, Bethesda, MD). Depressed and raised features were differentiated by scanning in the z-plane (vertical) with a Leica TCS SPS confocal microscope. Percent length of primary neurites on depressed and raised features was averaged for at least 100 randomly chosen neurites from each condition.

**2.8. Comparison of SGN Neurite Turning.** Neurite turns were measured using ImageJ primary neurite traces from immuno-fluorescent digital images that were captured as previously described. Trace data, containing X-Y neurite distance coordinates, was analyzed by measuring the angle of consecutive 10  $\mu\text{m}$  length neurite segments using Matlab. Neurite segment angle was measured relative to the horizontal plane. If three consecutive segments, that is, 30  $\mu\text{m}$  segment of the neurite, had a trajectory difference of at least 10° from the previous three consecutive segments then it was marked as a turning event. At least 50 neurites were scored for each pattern condition.

**2.9. Statistics.** Statistical analysis was performed using SigmaStat 3.5 software (Systat Software, Chicago, IL). A two-tailed *t* test was used to compare cellular alignment between unpatterned and patterned samples followed by a post hoc Mann-Whitney Rank Sum Test when normality criteria were not met. Multiple groups were compared by performing a one-way ANOVA followed by a post hoc Kruskal-Wallis analysis of variance on ranks and a Dunn's Method

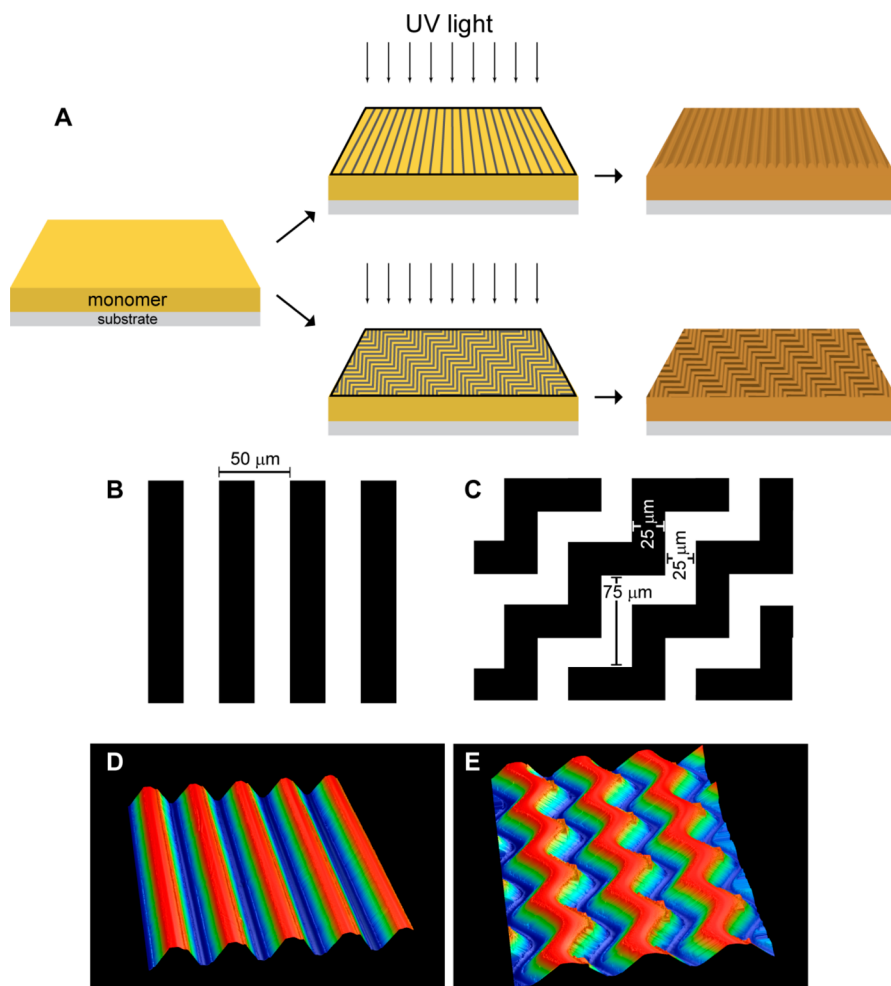


**Figure 1.** Schematic of micropattern fabrication process for neural pathfinding studies. (A) Photopolymerizable monomer is selectively exposed to UV light through a photomask resulting in micropatterns across the substrate surface. (B,C) Representation of transparent (white) and reflective (black) band size of the photomasks. (D,E) White light optical profiling 3D images of parallel and 90° angled micropatterned HMA-*co*-HDDMA substrates representing 100  $\mu\text{m}^2$  areas and channel amplitudes of 7  $\mu\text{m}$ .

multiple comparison procedure. Results were considered statistically significant if  $p < 0.05$ .

### 3. RESULTS AND DISCUSSION

**3.1. Photopolymerization of Uni- and Multidirectional Micropatterned Substrates.** To evaluate neural pathfinding behavior of SGN neurites, the inherent spatial and temporal control of photopolymerization were used to fabricate uni- and multidirectional micropattern substrates for contact guidance studies. Spatial control is achieved by masking the prepolymer formulation from initiating light and temporal control is afforded through shuttering of the light source at specific time increments. For a typical photoinitiated radical chain growth polymerization, a small concentration of photoinitiator in the prepolymer formulation absorbs photons and undergoes cleavage of a C–C bond that results in the generation of reactive free radicals. For this particular system, 2,2-dimethoxy-2-phenylacetophenone (DMPA) undergoes a Norrish type I reaction, that is, photochemical hemolysis of the  $\alpha$ -C–C bond of the ketone.<sup>47</sup> The free radical species then react with electron rich C–C double bonds on methacrylate moieties of the surrounding monomer which initiates the polymerization reaction. Propagation continues through polymerizable methacrylate groups until the growing kinetic chain is terminated via

recombination with another radical or through hydrogen abstraction and disproportionation. Because the rate of initiation for a photoinitiation reaction depends on absorbance of light, local reaction speeds can be modulated across a substrate surface by selectively masking incident irradiation.

Accordingly, unidirectional parallel line-space gratings were made by masking the prepolymer formulation with Ronchi rule optics that have alternating transparent (glass) and reflective (chrome) bands (Figure 1). Each band is a straight line with a width of 25  $\mu\text{m}$  and extends across the entire length of the mask. Multidirectional or angled patterns were generated by masking the reaction with repeating reflective angles. Masking the photopolymerization reaction in this manner locally modulates polymerization kinetics,<sup>48,49</sup> which results in microscale periodic raised and depressed features that match the width of the photomask bands. Surface depressions occur beneath reflective bands and raised features appear beneath transparent bands. Final thin film surface topography is composed of uniform, gradually transitioning microfeatures that contrast with stark, on–off type features generated via multistep lithographic etching methods.<sup>33,41,50</sup> The gradual transitions between microfeatures are likely due to the diffraction of light as it passes through microscale photomask bands<sup>51,52</sup> and due to diffusion of monomer toward reactive

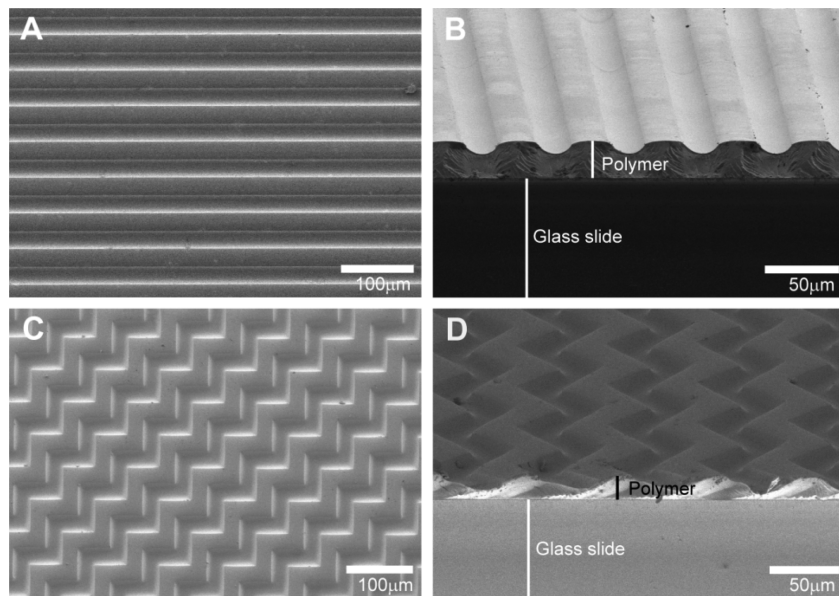


**Figure 2.** Representative SEM micrographs of micropatterned HMA-*co*-HDDMA thin films. (A) A top-down view of a parallel or unidirectional micropattern with a 50  $\mu\text{m}$  feature spacing and 7  $\mu\text{m}$  amplitude. (B) A tilted-cross sectional view of a parallel pattern demonstrating film thickness and gradual transitions between raised and depressed features. (C,D) Top-down and tilted-cross sectional views of repeating 90° angle or multidirectional micropattern with a 7  $\mu\text{m}$  amplitude.

regions as demonstrated in interference patterning holographic photopolymerization.<sup>53</sup> Once the light source is shuttered, the reaction rate rapidly decreases as no new radicals are generated via photon absorption.<sup>54</sup> Uni- and multidirectional micropatterns were measured and characterized by white light interferometry (Figure 1 D–E). As expected, micropattern spacing closely matches photomask band spacing.

For all substrates, the prepolymer formulation consisted of a 40 wt % hexyl methacrylate (HMA) and 59 wt % 1,6-hexanediol dimethacrylate (HDDMA) mixture with 1 wt % 2,2-dimethoxy-2-phenylacetophenone (DMPA) as the photoinitiator. In previous work, we demonstrated that poly(HMA-*co*-HDDMA) is sufficiently biocompatible to enable attachment, survival, and growth of SGNs under *in vitro* conditions.<sup>43</sup> We also illustrated that the comethacrylate can be photopatterned and that microfeature dimensions of the system are readily tunable by modulating photopolymerization parameters.<sup>41</sup>

**3.2. Photopolymerized Microfeature Morphology and Tuning.** Scanning electron microscopy (SEM) was used to characterize substrate morphology and to confirm white light interferometric measurements (Figure 2). For unidirectional patterns, continuous, 25  $\mu\text{m}$  wide parallel ridges and grooves run the length of the masked area with feature height remaining uniform across the surface. Multidirectional or repeating angle topographies also closely match microfabricated photomask band spacings with microfeatures spanning the entirety of the masked region. For both pattern types, photocured substrates have a film thickness of 18  $\mu\text{m}$  and a feature depth approximately 40% of the total thickness at  $7.4 \pm 0.7 \mu\text{m}$  for the given reaction conditions. Both patterns also have gradual transitions between raised and depressed features due to reactive species diffusion and diffraction of light during the photopolymerization.

Smooth transitions between photopolymerized microfeatures stand in contrast to infinite slope type features generated via etching lithographic methods. Cell–material interaction studies

on topographies fabricated by etching methods illustrate important cell behavior such as polarization and alignment along the axis of parallel features, differences in alignment to identical microfeatures based on cell type, and sensitivity to nanotopographical noise.<sup>55–57</sup> However, patterns without sharp features are advantageous for some studies in that they more closely mimic native cellular niche morphologies. They may also be used in physical-biochemical cue combination studies to prevent domination of contact guidance cues over biochemical signaling events. The single step photopolymerization of micropatterns is also advantageous because it is fast, low cost, and readily tunable between each sample run whereas etched features require a much longer multistep process, expensive reagents, and microfabrication equipment and different master templates for each desired feature height. Though, it should also be noted that direct, single step photopolymerization of micro- and nanotopography is limited in lateral feature resolution due to reactive species diffusion constraints and is also limited in ultimate feature depth based on monomer chemistry and reaction kinetics. Tuning of prepolymer formulation viscosity, photoinitiator choice, irradiation source, and monomer chemistries may mitigate, but likely will not eliminate, these potential disadvantages.

To compare neural pathfinding on both uni- and multidirectional patterns, microfeature amplitude was controlled by shuttering the photopolymerization reaction at specific UV exposure times (Figure 3). Polymerization rate rapidly decreases upon shuttering of the radiation source as no new radicals are formed to initiate propagation reactions and as existing radicals terminate by combination and disproportionation reactions. Temporal control of the reaction, thus afforded, enables kinetic trapping of specific microchannel amplitudes that allow for direct comparisons between pattern directionalities. To generate channel amplitudes of  $7.4 \pm 0.7 \mu\text{m}$  for both pattern types, UV light exposure was shuttered at 77 and 85 s for unidirectional and multidirectional patterns, respectively. Under the given reaction conditions, parallel

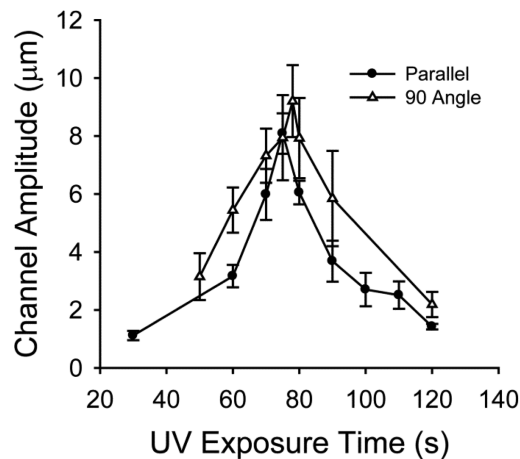


**Figure 3.** Channel amplitude is modulated by shuttering the UV light source at specific time increments. Feature depth for parallel and 90° angle patterns is similar at each exposure. Each point indicates mean  $\pm$  SD.

pattern amplitude ranged from approximately 1.3 to 8  $\mu\text{m}$  and 90° angle pattern amplitude ranged from 2 to 9  $\mu\text{m}$ . Amplitude profiles as a function of UV exposure time for both pattern types are very similar, with slight variations likely being attributable to differences in light diffraction patterns that alter incident light intensities locally at the substrate surface. Microfeature amplitude increase and subsequent decrease occur nearly symmetrically around a maximum amplitude UV exposure time step. Decreases in amplitude are likely due to backfilling of masked regions as reactive species diffuse into shadowed areas and as more photons are allowed to reach the

area through light diffraction and internal reflectance within the system.

**3.3. SGN Survival, Neurite Length, and Branching on Unpatterned and Patterned Substrates.** To compare differences in neurite behavior on varied directional surface cues, dissociated SGNs were cultured on unpatterned controls, unidirectional (parallel) patterns, and repeating angle (90° angle) patterns. Neuronal survival, neurite length, and branching were examined as an initial comparison (Figure 4). SGN survival on unpatterned and micropatterned poly(HMA-*co*-HDDMA) is comparable to survival on a tissue culture plastic (TCP) control ( $p > 0.05$ ). Further, no significant difference is evident between primary neurite length, i.e. the longest neurite from each neuron, on unpatterned controls compared to unidirectional micropatterns. Total neurite length, that is, primary neurite length plus branch length, on unpatterned and unidirectional substrates is also similar. However, both primary and total neurite lengths are approximately 20% shorter on repeating angle patterns, relative to unpatterned and parallel pattern substrates. Neurites on multidirectional surfaces may be shorter due to the presentation of a higher density of potential encounters with feature edges to the advancing neural growth cone compared to fewer such encounters on smooth or unidirectional surfaces. Each encounter with a feature edge is likely associated with growth cone stalling and the underlying focal adhesion formation or removal and cytoskeleton rearrangement events which reduce the rate of neurite extension.<sup>58</sup>

In addition to neurite length, SGN neurite branching also significantly differs on substrates with varied physical surface cues. The degree of branching per neurite and per 100  $\mu\text{m}$  of neurite length is lowest for SGNs cultured on unpatterned

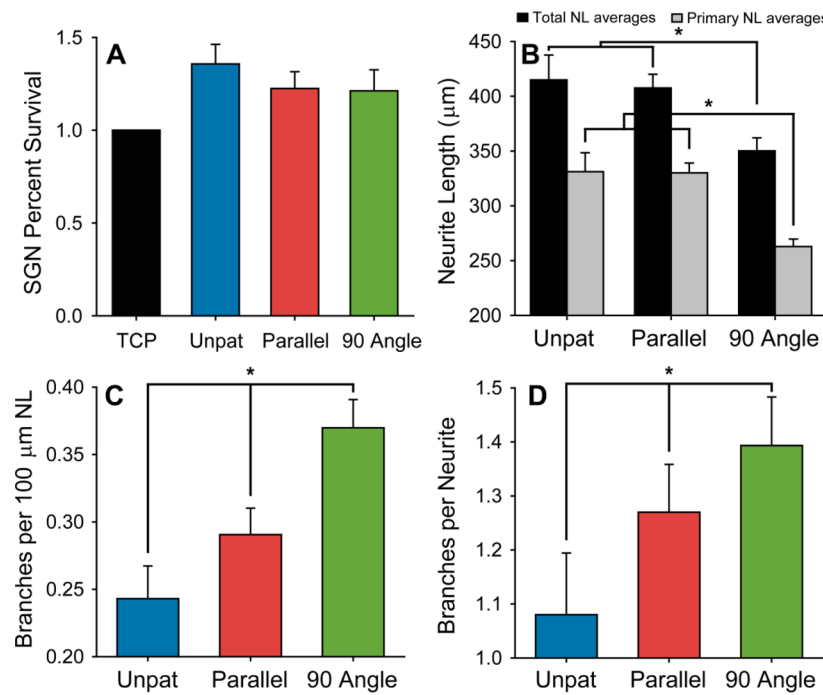


**Figure 4.** SGN survival, total and primary neurite length (NL), and branching on unpatterned controls and on parallel and 90° angle micropatterns of HMA-*co*-HDDMA polymer substrates. (A) SGN survival on unpatterned and micropatterned substrates normalized to a tissue culture plastic (TCP) control. (B) Total and primary SGN neurite lengths are significantly shorter than corresponding lengths on parallel patterns and unpatterned controls (\* $p < 0.05$ , ANOVA). (C–D) Significantly more branches per neurite length and per neurite on 90° angle patterns are observed compared to neurites on parallel patterns and unpatterned controls (\* $p < 0.05$ , ANOVA). Error bars represent standard error of the mean (SE).

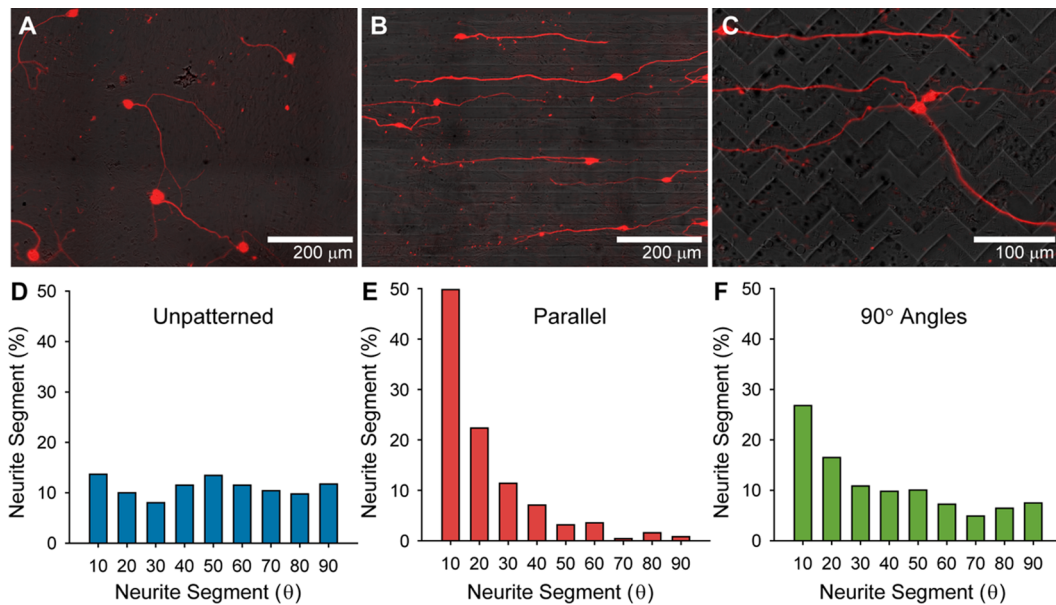


**Figure 5.** SGN neurite alignment on variations in topographic cues. (A–C) Immunofluorescent images of neurite growth from dissociated SGNs on unpatterned (A), parallel (B), and 90° angle (C) substrates. (D–F) Distribution of SGN neurite segment angles relative to the horizontal plane on unpatterned (D), parallel (E), and 90° angle (F) substrates. Regenerative neurite growth orients randomly on unpatterned substrates as evidenced by a nearly equal distribution of neurite segment angles relative to the horizontal plane. Neurites strongly align to unidirectional topographic cues with 70% of the neurite segment angles at or below 20° from the pattern direction. Neurites on repeating 90° angle patterns do not closely track multidirectional cues as demonstrated by the low incidence of 45° angle neurite segments. They do align somewhat to the horizontal plane, although with a broader distribution of angles than on parallel patterns. Dissociated cultures were stained with anti-NF200 antibodies. Micropatterned substrates have a channel amplitude of 7  $\mu\text{m}$ .

substrates. Branching increases on patterned surfaces, suggesting that growth cone encounters with pattern edges induce neurite branch formation. Neurite branching is highest on multidirectional features with a 52% increase in branches per neurite length compared to unpatterned controls. Interestingly, the neurite length and branching results taken together illustrate that neural processes behave differently on physical cues with varied directionality even when all other experimental conditions are held constant including the width and height of the microfeatures.

**3.4. SGN Neurite and SGSC Alignment on Unpatterned and Uni- and Multidirectional Substrates.** Developing precise spatial control of de novo neurite growth from neurons that are relevant to neural prosthetics, such as inner ear SGNs, will lead to enhanced prosthesis performance and improved functional outcomes for patients. Directing neurite growth in this manner will require multiple types of biologically actionable cues including biophysical cues that can either induce or inhibit neurite turning events. Accordingly, to compare neurite pathfinding ability on varied biophysical cues, SGNs were cultured on unpatterned, unidirectional, and multidirectional photopolymerized substrates (Figure 5). Qualitative immunofluorescence imaging illustrates that SGN neurite outgrowth extends randomly on unpatterned substrates with unpredictable turning events. Conversely, neurites on unidirectional patterns are observed to strongly orient to and grow parallel to the microfeature direction (horizontal) while exhibiting few if any turning events per neurite (Figure 5B). Interestingly, while SGN neurites on multidirectional patterns do not extend randomly, they also do not closely track the repeating sequence of 90° turning cues along a micropattern path despite encountering physical microfeatures that are comparable in width and depth to those of the unidirectional

patterns (Figure 5C). Rather, extending neurites are often observed to align horizontally and elongate down the length of a feature path. It is interesting that the neurites extend in this fashion, even though they must cross multiple feature transitions near the angle turning points. Furthermore, neurites on multidirectional patterns also turn much more frequently than on unidirectional substrates with the accompanying behavior of crossing over a sequence of microfeatures prior to realigning to the horizontal plane. These microfeature crossing events are rare in the case of neurite growth on unidirectional patterns, especially over multiple transitions.

Qualitative SGN neurite alignment observations are further supported by sectioning equal lengths of neurite segments for all scored neurites and measuring their alignment angle relative to the horizontal plane (Figure 5D–F). Neurite segment angles ( $\leq 90^\circ$ ) are binned as a percentage of the total neurite segments measured in 10° increments to represent overall alignment. SGN neurites on unpatterned polymer substrates extend randomly as demonstrated by the relatively equal distribution of neurite segment angles across the 0–90° spectrum of alignment. In contrast, neurite segment angles are much more frequent at low angles (i.e.,  $< 20^\circ$ ) relative to horizontal on unidirectional, parallel feature micropatterns. Approximately 50% of the neurite segments are considered completely aligned to the pattern direction with an alignment angle of 10° or less and a full 72% of the neurite segment population is within the 20° angle population, indicating significant alignment to pattern features.

However, as previously mentioned, neurites on multidirectional substrates do not strongly track the repeating 90° angle patterns as evidenced by low incidence (~20%) of neurite segment angles in the 40° and 50° degree bins. Because the 90° angle features have been rotated 45° for imaging, it could be

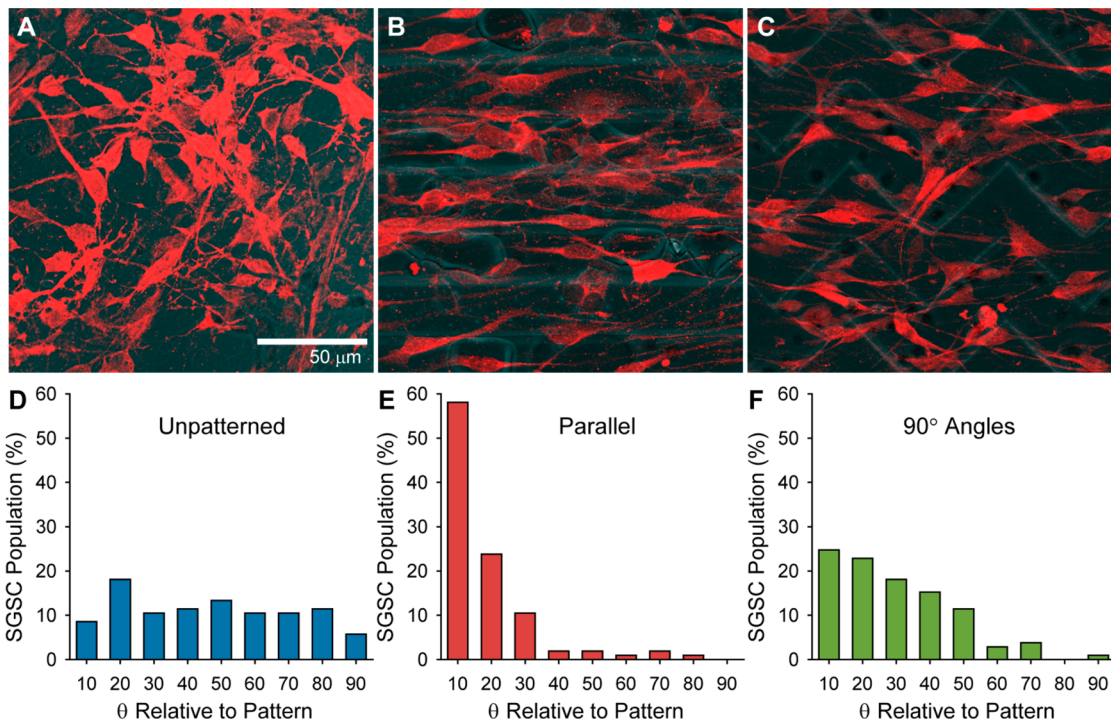


**Figure 6.** SGSC alignment on variations in topographic cues. (A–C) Immunofluorescent images of SGSCs on unpatterned (A), parallel (B), and 90° angle (C) substrates. (D–F) Distribution of SGSC angles relative to the horizontal plane on unpatterned (D), parallel (E), and 90° angle (F) substrates. SGSCs orient randomly on unpatterned substrates and align strongly to unidirectional topographic cues with 80% of the cell angles at or below 20° from the pattern direction. SGSCs on repeating 90° angle patterns do not closely track multidirectional cues as demonstrated by the low incidence of 45° cellular angles. Dissociated cultures were stained with anti-S100 antibodies. Micropatterned substrates have a channel amplitude of 7  $\mu\text{m}$ .

expected, assuming that neurite growth is strongly and consistently influenced by micropattern physical features on this size scale, that a significant incidence of neurite segment angles at or near 45° relative to the horizontal plane would be evident. Instead, a fairly equal distribution exists across all segment angles in the 30–90° population with a relatively high incidence (43%) of neurite segments at or below 20° from the horizontal plane. Importantly, the parallel and repeating angle micropatterns used for both experiments are quite similar. In both cases, the ridge and groove widths are 25  $\mu\text{m}$  and the channel amplitude or feature height is approximately 7  $\mu\text{m}$ . Polymerization was halted at similar time steps for both platforms by shutting off the UV light source yielding very similar groove-ridge transitions. All else being equal, it might be expected to see SGN neurites closely tracking the groove paths and, while perhaps not making exact 90° angle turns, there would still be a high incidence of 45° angle neurite segments tracking the groove path. It is clear that the neurite segment distribution does not match the random distribution seen on unpatterned polymer substrates but that it more closely resembles neurite orientation on unidirectional platforms. However, despite the similarities in neurite alignment to unidirectional patterns, outgrowth complexity increases on multidirectional substrates as neurites are observed to change direction and to cross microfeatures significantly more than on comparable unidirectional features.

To realize functional outcome improvements of neural prosthetics, it may be crucial to direct neurites to specific but separate areas that contain stimulating electrodes.<sup>20</sup> While a variety of neural contact guidance studies demonstrate strong alignment to the long axis of parallel feature micropatterns,

their use may be limited to applications that require significant unidirectional growth such as intraluminal patterning of nerve conduits to bridge nerve gaps.<sup>8</sup> Appropriate turning events will be required to spatially segregate and then stimulate specific neurites or groups of neurites. Multidirectional patterns with repeating 90° turns in this work induced greater turning than unidirectional patterns, though neurites are not observed to turn at each encounter of a biophysical cue. Similar behavior occurs when neurites extend between appropriately spaced microposts.<sup>59–61</sup> A lower density in directional changes per area or turns with wider angles may allow for more consistent guidance and predictable turning events throughout the length of a neurite.

Because glial cells are crucial to the proper function and survival of neuronal cells and because they support and direct neurite growth,<sup>43,62,63</sup> the behavior and alignment of SGSCs was also measured and compared on unpatterned and uni- and multidirectional micropatterns (Figure 6). SGSC alignment mirrors SGN neurite segment alignment. In this case, each scored SGSC was fit with an ellipse and the alignment was measured as the angle between the major axis of the ellipse relative to the horizontal plane. SGSCs orient randomly on unpatterned substrates and strongly align to parallel, unidirectional micropatterns with 82% of SGSCs having an alignment angle of 20° or less. As with SGN neurites on multidirectional platforms, SGSCs do not orient randomly as if on an unpatterned surface but more closely resemble horizontally aligned growth as seen on parallel micropatterns. Again, there is a much lower incidence of 45° alignment angles than would be expected if SGSCs closely tracked repeating 90° angle microfeatures.

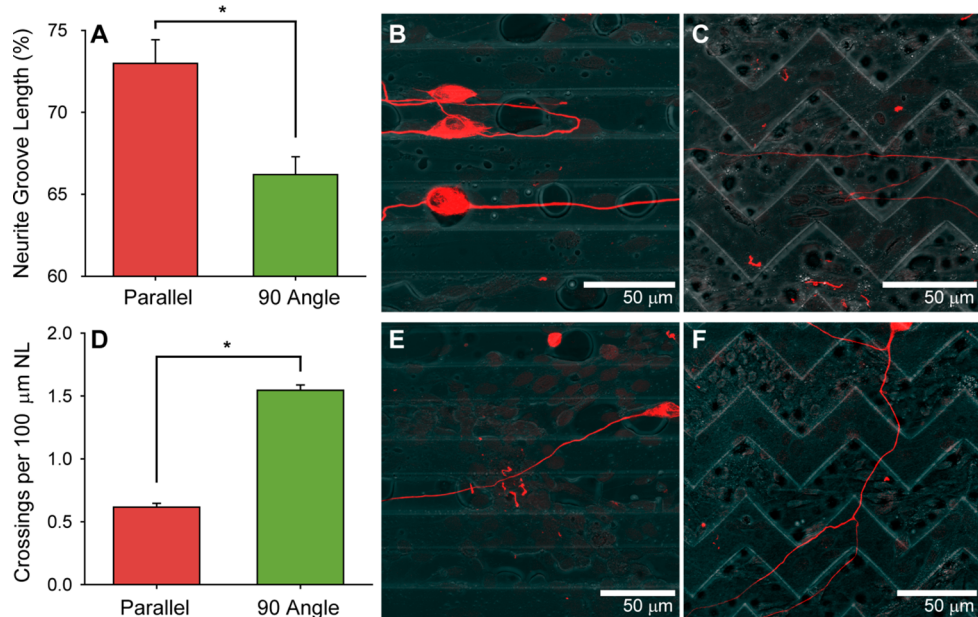


**Figure 7.** SGN percent neurite length in depressed microfeatures and feature crossing per neurite length on uni- and multidirectional topographic cues. (A) The majority of SGN neurite length on both parallel and 90° angle patterns is located in the grooves (\* $p < 0.05$ , Mann–Whitney Rank Sum test). (B,C) Immunofluorescent images of SGN neurite growth in groove microfeatures. (D) SGN neurites crossed ridge-groove transitions significantly more on multidirectional patterns compared to unidirectional substrates (\* $p < 0.05$ , Mann–Whitney Rank Sum test). (E,F) Immunofluorescent images of SGN neurites crossing ridge-groove transitions on various micropatterns. Dissociated cultures were stained with anti-NF200 antibodies. Micropatterned substrates have a channel amplitude of 7  $\mu\text{m}$ .

**3.5. SGN Neurite Positioning and Microfeature Crossing.** The percentage of neurite length in microfeature grooves and the number of feature crossings per neurite length were measured to further characterize differences in neural pathfinding on uni- versus multidirectional surface cues (Figure 7). The majority of regenerative SGN neurite length is found in depressed microfeatures (i.e., grooves) on both parallel and repeating angle micropatterns. Nearly 75% of all neurite length tracks surface depressions when SGNs are cultured on parallel feature micropatterns. A few neurites were even observed to turn 180° while remaining sequestered within microgrooves (Figure 7B). The quantified preference for depressed features is in contrast to other research, which observed neural processes preferentially growing on elevated features; however, the width of the features used were much narrower (i.e.,  $< 1 \mu\text{m}$ ) than the photopolymerized patterns used here.<sup>14</sup> While the majority of neurite length on 90° angle patterns is also found in surface depressions, the percent length in the depressions is still significantly less than that of neurites on unidirectional features. The difference is likely due to the presentation of multiple directional cues to the advancing growth cone, which increases the number of potential guidance points, and ultimately leads to increased topographic feature crossings.

A crossing event for this study is defined as the transition of the primary neurite from a raised or depressed microfeature to its corresponding opposite. Due to strong alignment on parallel microfeatures, SGN neurite crossing is, on average, very low with many neurites making only one or no feature crossings throughout the entirety of their length. Conversely, microfeature crossings per neurite length on multidirectional patterns are significantly higher than on unidirectional patterns. Approximately three times the number of crossing events per length of neurite are observed on multidirectional micropatterns (Figure 7 D–F). Therefore, despite microfeatures for

both pattern types having nearly identical widths and depths, SGN neurite pathfinding does not consistently track every change in feature direction as pattern complexity increases. Rather, neurites appear to extend in a manner that minimizes turning events by growing either down the length of a groove path (i.e., horizontally) or directly over multiple feature transitions.

**3.6. SGN Neurite Turning on Unpatterned and Uni- and Multidirectional Substrates.** The number of turns per neurite in response to topographic guidance cues was measured as a final comparison of SGN neurite pathfinding ability on uni- and multidirectional patterns and on unpatterned controls (Figure 8). Turns are defined as a 10° change in direction over three consecutive 10  $\mu\text{m}$  length neurite segments relative to the previous three segments. Ultimately, the capacity to guide regenerative neurite growth to spatially specific stimulating

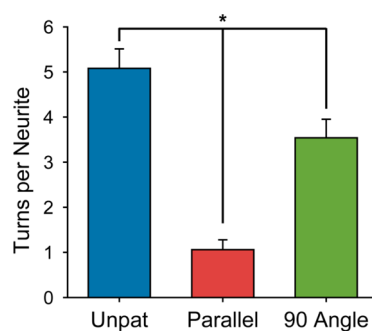


**Figure 8.** Number of turns per SGN neurite on substrates with varied topography. SGN neurites turned significantly more on unpatterned surfaces compared to patterned substrates and on patterns that change direction compared to unidirectional morphologies (\* $p < 0.05$ , ANOVA).

elements will require strong adherence to engineered guidance cues and may include precision turning at specific points. SGN neurites turn over five times more on unpatterned substrates compared to unidirectional micropatterns. They also turn significantly more on unpatterned substrates compared to neurites on repeating angle features. The high degree of turning on unpatterned platforms supports the observation that neurite growth is random on unpatterned controls and results in multiple instances of neural growth cone direction change and, thus, turning points for any given neurite (Figure 5).

The comparatively low number of neurite turns on unidirectional patterns confirms the strong neural alignment data on parallel microfeatures and further supports the observation that there is little to no feature crossing for a given neurite on unidirectional guidance cues. However, while significantly more turning events are evident on multidirectional patterns compared to unidirectional features, the neurites do not closely track each 90° turn but can cross over multiple microfeatures and turn to align along portions of them along its path length.

#### 4. CONCLUSION

Directing regenerative neural pathfinding with engineered surface cues to specific stimulatory elements will potentially improve the neural-prosthesis interface and lead to enhanced functional outcomes. In this work, we evaluate the neural pathfinding ability of SGN neurites on multidirectional micropatterns generated using the spatial and temporal control inherent to photopolymerization. Microfeature shape and width are controlled through photomask design, and feature depth is tuned on the micrometer scale by altering reaction parameters of the photopolymerization. The pathfinding ability of SGNs was evaluated on multidirectional repeating 90° patterns and compared to behavior on unpatterned, and unidirectional micropatterns. SGN neurites extend randomly on unpatterned surfaces and strongly align to and consistently track unidirectional patterns. Interestingly, when presented with multidirectional cues of the same width and height as those of the unidirectional pattern, SGN neurites are substantially influenced by, but do not consistently track, repeating turns. Rather, neurite extension is observed to avoid turning events even to the extent of crossing over multiple feature transitions which is rarely seen on unidirectional patterns. Spiral ganglion Schwann cells (SGSCs), which provide trophic support to SGNs, mirror the alignment behavior of SGN neurites on each pattern type. On both uni- and multidirectional patterns, the majority of the neurite path length is located in depressed surface features but significantly more feature crossing events occur on multidirectional surfaces. This work improves understanding of neural pathfinding from prosthesis-relevant neurons in relation to physical guidance cues and informs efforts to direct neurite growth toward specific stimulatory elements for the purpose of improving functional outcomes of neural prosthetics. Precisely directing neurite growth in this manner will enable fabrication of next generation neural prosthetics with enhanced stimulatory specificity.

#### AUTHOR INFORMATION

##### Corresponding Author

\*Email: allan-guymon@uiowa.edu Tel: (319)335-5015.

##### Notes

The authors declare no competing financial interest.

#### ACKNOWLEDGMENTS

The authors acknowledge funding support from the National Science Foundation (CBET-0933450), the National Institutes of Health (NCRR-UL1RR024979, NIDCD-P30 DC010362, and NIDCD R01DC012578), and the American Hearing Research Foundation. We also acknowledge government support from the Department of Defense, Air Force Office of Scientific Research, for a National Defense Science and Engineering Graduate (NDSEG) Fellowship, 32 CFR 168a.

#### REFERENCES

- (1) Mata, A.; Kim, E. J.; Boehm, C. A.; Fleischman, A. J.; Muschler, G. F.; Roy, S. A Three-Dimensional Scaffold with Precise Micro-architecture and Surface Micro-textures. *Biomaterials* **2009**, *30*, 4610–4617.
- (2) Kubo, K.; Att, W.; Yamada, M.; Ohmi, K.; Tsukimura, N.; Suzuki, T.; Maeda, H.; Ogawa, T. Microtopography of Titanium Suppresses Osteoblastic Differentiation but Enhances Chondroblastic Differentiation of Rat Femoral Periosteum-Derived Cells. *J. Biomed Mater. Res. A* **2008**, *87A*, 380–391.
- (3) Yim, E. K.; Pang, S. W.; Leong, K. W. Synthetic Nanostructures Inducing Differentiation of Human Mesenchymal Stem Cells into Neuronal Lineage. *Exp. Cell Res.* **2007**, *313*, 1820–1829.
- (4) Engler, A. J.; Sen, S.; Sweeney, H. L.; Discher, D. E. Matrix Elasticity Directs Stem Cell Lineage Specification. *Cell* **2006**, *126*, 677–689.
- (5) Hoffman-Kim, D.; Mitchel, J. A.; Bellamkonda, R. V. Topography, Cell Response, and Nerve Regeneration. *Annu. Rev. Biomed. Eng.* **2010**, *12*, 203–231.
- (6) Spivey, E. C.; Khaing, Z. Z.; Shear, J. B.; Schmidt, C. E. The Fundamental Role of Subcellular Topography in Peripheral Nerve Repair Therapies. *Biomaterials* **2012**, *33*, 4264–4276.
- (7) Straley, K. S.; Foo, C. W.; Heilshorn, S. C. Biomaterial Design Strategies for the Treatment of Spinal Cord Injuries. *J. Neurotrauma* **2010**, *27*, 1–19.
- (8) Daly, W.; Yao, L.; Zeugolis, D.; Windebank, A.; Pandit, A. Biomaterials Approach to Peripheral Nerve Regeneration: Bridging the Peripheral Nerve Gap and Enhancing Functional Recovery. *J. R Soc. Interface* **2012**, *9*, 202–221.
- (9) Hurtado, A.; Cregg, J. M.; Wang, H. B.; Wendell, D. F.; Oudega, M.; Gilbert, R. J.; McDonald, J. W. Robust CNS Regeneration after Complete Spinal Cord Transection using Aligned Poly-L-lactic Acid Microfibers. *Biomaterials* **2011**, *32*, 6068–6079.
- (10) Oliva, A. A.; James, C. D.; Kingman, C. E.; Craighead, H. G.; Bunker, G. A. Patterning Axonal Guidance Molecules Using a Novel Strategy for Microcontact Printing. *Neurochem. Res.* **2003**, *28*, 1639–1648.
- (11) Gustavsson, P.; Johansson, F.; Kanje, M.; Wallman, L.; Linsmeier, C. E. Neurite Guidance on Protein Micropatterns Generated by a Piezoelectric Microdispenser. *Biomaterials* **2007**, *28*, 1141–1151.
- (12) Schmalenberg, K. E.; Uhrich, K. E. Micropatterned Polymer Substrates Control Alignment of Proliferating Schwann Cells to Direct Neuronal Regeneration. *Biomaterials* **2005**, *26*, 1423–1430.
- (13) Branch, D. W.; Wheeler, B. C.; Brewer, G. J.; Leckband, D. E. Long-Term Stability of Grafted Polyethylene Glycol Surfaces for use with Microstamped Substrates in Neuronal Cell Culture. *Biomaterials* **2001**, *22*, 1035–1047.
- (14) Johansson, F.; Carlberg, P.; Danielsen, N.; Montelius, L.; Kanje, M. Axonal Outgrowth on Nano-imprinted Patterns. *Biomaterials* **2006**, *27*, 1251–1258.
- (15) Miller, C.; Jeftinija, S.; Mallapragada, S. Synergistic Effects of Physical and Chemical Guidance Cues on Neurite Alignment and Outgrowth on Biodegradable Polymer Substrates. *Tissue Eng.* **2002**, *8*, 367–378.

- (16) Wittig, J. H.; Ryan, A. F.; Asbeck, P. M. A Reusable Microfluidic Plate with Alternate-Choice Architecture for Assessing Growth Preference in Tissue Culture. *J. Neurosci. Methods* **2005**, *144*, 79–89.
- (17) Yao, L.; Pandit, A.; Yao, S.; McCaig, C. D. Electric Field-Guided Neuron Migration: A Novel Approach in Neurogenesis. *Tissue Eng. Part B Rev.* **2011**, *17*, 143–153.
- (18) Koh, H. S.; Yong, T.; Teo, W. E.; Chan, C. K.; Puhaindran, M. E.; Tan, T. C.; Lim, A.; Lim, B. H.; Ramakrishna, S. In Vivo Study of Novel Nanofibrous Intra-luminal Guidance Channels to Promote Nerve Regeneration. *J. Neural Eng.* **2010**, *7*, 046003.
- (19) Richardson, J. A.; Rementer, C. W.; Bruder, J. M.; Hoffman-Kim, D. Guidance of Dorsal Root Ganglion Neurites and Schwann Cells by Isolated Schwann Cell Topography on Poly(dimethyl siloxane) Conduits and Films. *J. Neural Eng.* **2011**, *8*, 046015.
- (20) O'Leary, S. J.; Richardson, R. R.; McDermott, H. J. Principles of Design and Biological Approaches for Improving the Selectivity of Cochlear Implant Electrodes. *J. Neural Eng.* **2009**, *6*, 055002.
- (21) Leach, J. B.; Achyuta, A. K.; Murthy, S. K. Bridging the Divide Between Neuroprosthetic Design, Tissue Engineering, and Neurobiology. *Front. Neuroeng.* **2010**, *2*, 18.
- (22) Winter, J. O.; Cogan, S. F.; Rizzo, J. Retinal Prostheses: Current Challenges and Future Outlook. *J. Biomater. Sci. Polym. Ed.* **2007**, *18*, 1031–1055.
- (23) Shannon, R. V.; Fu, Q. J.; Galvin, J. The Number of Spectral Channels Required for Speech Recognition Depends on the Difficulty of the Listening Situation. *Acta Otolaryngol. Suppl.* **2004**, *552*, 50–54.
- (24) Rubinstein, J. T. How Cochlear Implants Encode Speech. *Curr. Opin. Otolaryngol. Head Neck Surg.* **2004**, *12*, 444–8.
- (25) Leng, T.; Wu, P.; Mehenti, N. Z.; Bent, S. F.; Marmor, M. F.; Blumenkranz, M. S.; Fishman, H. A. Directed Retinal Nerve Cell Growth for use in a Retinal Prosthesis Interface. *Invest. Ophthalmol. Visual Sci.* **2004**, *45*, 4132–4137.
- (26) Evans, A. J.; Thompson, B. C.; Wallace, G. G.; Millard, R.; O'Leary, S. J.; Clark, G. M.; Shepherd, R. K.; Richardson, R. T. Promoting Neurite Outgrowth from Spiral Ganglion Neuron Explants using Polypyrrole/BDNF-Coated Electrodes. *J. Biomed Mater. Res. A* **2009**, *91A*, 241–250.
- (27) Brors, D.; Aletsee, C.; Schwager, K.; Mlynki, R.; Hansen, S.; Schäfers, M.; Ryan, A. F.; Dazert, S. Interaction of Spiral Ganglion Neuron Processes with Alloplastic Materials In Vitro. *Hear. Res.* **2002**, *167*, 110–121.
- (28) Mehenti, N. Z.; Peterman, M. C.; Leng, T.; Marmor, M. F.; Blumenkranz, M. S.; Bent, S. F. A Retinal Interface Based on Neurite Micropatterning for Single Cell Stimulation. *Invest. Ophthalmol. Visual Sci.* **2003**, *44*, U704–U704.
- (29) Roehm, P. C.; Hansen, M. R. Strategies to Preserve or Regenerate Spiral Ganglion Neurons. *Curr. Opin. Otolaryngol. Head Neck Surg.* **2005**, *13*, 294–300.
- (30) Guenther, E.; Troger, B.; Schlosshauer, B.; Zrenner, E. Long-Term Survival of Retinal Cell Cultures on Retinal Implant Materials. *Vision Res.* **1999**, *39*, 3988–3994.
- (31) Cui, X. Y.; Wiler, J.; Dzaman, M.; Altschuler, R. A.; Martin, D. C. In Vivo Studies of Polypyrrole/Peptide Coated Neural Probes. *Biomaterials* **2003**, *24*, 777–787.
- (32) Teixeira, A. I.; Abrams, G. A.; Bertics, P. J.; Murphy, C. J.; Nealey, P. F. Epithelial Contact Guidance on Well-Defined Micro- and Nanostructured Substrates. *J. Cell. Sci.* **2003**, *116*, 1881–1892.
- (33) Hsu, S.; Lu, P. S.; Ni, H.; Su, C. Fabrication and Evaluation of Microgrooved Polymers as Peripheral Nerve Conduits. *Biomed. Microdevices* **2007**, *9*, 665–674.
- (34) Song, M.; Uhrich, K. E. Optimal Micropattern Dimensions Enhance Neurite Outgrowth Rates, Lengths, and Orientations. *Ann. Biomed. Eng.* **2007**, *35*, 1812–1820.
- (35) Rajnicek, A. M.; Britland, S.; McCaig, C. D. Contact Guidance of CNS Neurites on Grooved Quartz: Influence of Groove Dimensions, Neuronal Age and Cell Type. *J. Cell. Sci.* **1997**, *110*, 2905–2913.
- (36) Baek, N. S.; Kim, Y. H.; Han, Y. H.; Lee, B. J.; Kim, T.; Kim, S.; Choi, Y.; Kim, G. H.; Chung, M.; Jung, S. Facile Photopatterning of Polyfluorene for Patterned Neuronal Networks. *Soft Matter* **2011**, *7*, 10025–10031.
- (37) Sun, T.; Kovac, J.; Voldman, J. Image-Based Single-Cell Sorting via Dual-Polymerized Microwell Arrays. *Anal. Chem.* **2014**, *86*, 977–981.
- (38) Hao, Y.; Shih, H.; Muñoz, Z.; Kemp, A.; Lin, C. Visible Light Cured Thiol-Vinyl Hydrogels with Tunable Degradation for 3D Cell Culture. *Acta Biomater.* **2014**, *10*, 104–114.
- (39) Nichol, J. W.; Koshy, S. T.; Bae, H.; Hwang, C. M.; Yamanlar, S.; Khademhosseini, A. Cell-Laden Microengineered Gelatin Methacrylate Hydrogels. *Biomaterials* **2010**, *31*, 5536–5544.
- (40) Hume, P. S.; Anseth, K. S. Inducing local T Cell Apoptosis with Anti-Fas-Functionalized Polymeric Coatings Fabricated via Surface-Initiated Photopolymerizations. *Biomaterials* **2010**, *31*, 3166–3174.
- (41) Tuft, B. W.; Li, S.; Xu, L.; Clarke, J. C.; White, S. P.; Guymon, B. A.; Perez, K. X.; Hansen, M. R.; Guymon, C. A. Photopolymerized Microfeatures for Directed Spiral Ganglion Neurite and Schwann Cell Growth. *Biomaterials* **2013**, *34*, 42–54.
- (42) Jeon, E.; Xu, N.; Xu, L.; Hansen, M. R. Influence of Central Glia on Spiral Ganglion Neuron Neurite Growth. *Neuroscience* **2011**, *177*, 321–334.
- (43) Hansen, M. R.; Vijapurkar, U.; Koland, J. G.; Green, S. H. Reciprocal Signaling Between Spiral Ganglion Neurons and Schwann Cells Involves Neuregulin and Neurotrophins. *Hear. Res.* **2001**, *161*, 87–98.
- (44) Hegarty, J.; Kay, A.; Green, S. Trophic Support of Cultured Spiral Ganglion Neurons by Depolarization Exceeds and is Additive with that by Neurotrophins or cAMP and Requires Elevation of [Ca<sup>2+</sup>]<sub>i</sub> within a Set Range. *J. Neurosci.* **1997**, *17*, 1959–1970.
- (45) Roehm, P. C.; Xu, N.; Woodson, E. A.; Green, S. H.; Hansen, M. R. Membrane Depolarization Inhibits Spiral Ganglion Neurite Growth via Activation of Multiple Types of Voltage Sensitive Calcium Channels and Calpain. *Mol. Cell Neurosci.* **2008**, *37*, 376–387.
- (46) Clarke, J. C.; Tuft, B. W.; Clinger, J. D.; Levine, R.; Figueiroa, L. S.; Allan Guymon, C.; Hansen, M. R. Micropatterned Methacrylate Polymers Direct Spiral Ganglion Neurite and Schwann Cell Growth. *Hear. Res.* **2011**, *278*, 96–105.
- (47) Jaegermann, P.; Lendzian, F.; Rist, G.; Möbius, K. Time-Resolved ESR and Endor During the Photolysis of  $\omega,\omega$ -Dimethoxy- $\omega$ -Phenyl-Acetophenone. *Chem. Phys. Lett.* **1987**, *140*, 615–619.
- (48) Bryant, S. J.; Hauch, K. D.; Ratner, B. D. Spatial Patterning of Thick Poly(2-hydroxyethyl methacrylate) Hydrogels. *Macromolecules* **2006**, *39*, 4395–4399.
- (49) Bryant, S. J.; Cuy, J. L.; Hauch, K. D.; Ratner, B. D. Photo-Patterning of Porous Hydrogels for Tissue Engineering. *Biomaterials* **2007**, *28*, 2978–2986.
- (50) Mattotti, M.; Alvarez, Z.; Ortega, J. A.; Planell, J. A.; Engel, E.; Alcántara, S. Inducing Functional Radial Glia-like Progenitors from Cortical Astrocyte Cultures using Micropatterned PMMA. *Biomaterials* **2012**, *33*, 1759–1770.
- (51) Abbe, E. Contributions to the Theory of the Microscope and the Microscopic Perception. *Arch. Mikr. Anat.* **1873**, *9*, 413–468.
- (52) Garini, Y.; Vermolen, B. J.; Young, I. T. From Micro to Nano: Recent Advances in High-Resolution Microscopy. *Curr. Opin. Biotechnol.* **2005**, *16*, 3–12.
- (53) Smith, D. M.; Li, C. Y.; Bunning, T. J. Light-Directed Mesoscale Phase Separation via Holographic Polymerization. *J. Polym. Sci., Part B: Polym. Phys.* **2014**, *52*, 232–250.
- (54) Odian, G. *Principles of Polymerization*, 4th ed; John Wiley & Sons Inc: Hoboken, NJ, 2004; pp 264–271.
- (55) Hsu, S. H.; Chen, C. Y.; Lu, P. S.; Lai, C. S.; Chen, C. J. Oriented Schwann Cell Growth on Microgrooved Surfaces. *Biotechnol. Bioeng.* **2005**, *92*, 579–588.
- (56) Biela, S. A.; Su, Y.; Spatz, J. P.; Kemkemer, R. Different Sensitivity of Human Endothelial Cells, Smooth Muscle Cells, and Fibroblasts to Topography in the Nano–Micro Range. *Acta Biomater.* **2009**, *5*, 2460–2466.

- (57) Jacchetti, E.; Di Renzo, C.; Meucci, S.; Nocchi, F.; Beltram, F.; Cecchini, M. Wharton's Jelly Human Mesenchymal Stem Cell Contact Guidance by Noisy Nanotopographies. *Sci. Rep.* **2014**, *4*, 3830.
- (58) Neubrand, V. E.; Thomas, C.; Schmidt, S.; Debant, A.; Schiavo, G. Kidins220/ARMS Regulates Rac1-Dependent Neurite Outgrowth by Direct Interaction with the RhoGEF Trio. *J. Cell Sci.* **2010**, *123*, 2111–2123.
- (59) Micholt, L.; Gartner, A.; Prodanov, D.; Braeken, D.; Dotti, C. G.; Bartic, C. Substrate Determines Neuronal Polarization and Growth In Vitro. *PLoS One* **2013**, *8*, e66170.
- (60) Dowell-Mesfin, N. M.; Abdul-Karim, M.; Turner, A. M.; Schanz, S.; Craighead, H. G.; Roysam, B.; Turner, J. N.; Shain, W. Topographically Modified Surfaces Affect Orientation and Growth of Hippocampal Neurons. *J. Neural Eng.* **2004**, *1*, 78–90.
- (61) Kundu, A.; Micholt, L.; Friedrich, S.; Rand, D. R.; Bartic, C.; Braeken, D.; Levchenko, A. Superimposed Topographic and Chemical Cues Synergistically Guide Neurite Outgrowth. *Lab Chip* **2013**, *13*, 3070–3081.
- (62) Davies, A. M. Neuronal Survival: Early Dependence on Schwann Cells. *Curr. Biol.* **1998**, *8*, R15–R18.
- (63) Morris, J. K.; Lin, W.; Hauser, C.; Marchuk, Y.; Getman, D.; Lee, K. Rescue of the Cardiac Defect in ErbB2Mutant Mice Reveals Essential Roles of ErbB2 in Peripheral Nervous System Development. *Neuron* **1999**, *23*, 273–283.